

We are IntechOpen, the world's leading publisher of Open Access books Built by scientists, for scientists

4,800

Open access books available

122,000

International authors and editors

135M

Downloads

Our authors are among the

154

Countries delivered to

TOP 1%

most cited scientists

12.2%

Contributors from top 500 universities



WEB OF SCIENCE™

Selection of our books indexed in the Book Citation Index
in Web of Science™ Core Collection (BKCI)

Interested in publishing with us?
Contact book.department@intechopen.com

Numbers displayed above are based on latest data collected.
For more information visit www.intechopen.com



Fatigue Limit Reliability Analysis for Notched Material with Some Kinds of Dense Inhomogeneities Using Fracture Mechanics

Tatsujiro Miyazaki, Shigeru Hamada and Hiroshi Noguchi

Abstract

This study proposes a quantitative method for predicting fatigue limit reliability of a notched metal containing inhomogeneities. Since the fatigue fracture origin of the notched metal cannot be determined in advance because of stress nonuniformity, randomly distributed particles, and scatter of a matrix, it is difficult to predict the fatigue limit. The present method utilizes a stress-strength model incorporating the “statistical hardness characteristics of a matrix under small indentation loads” and the “statistical hardness characteristics required for non-propagation of fatigue cracks from microstructural defects”. The notch root is subdivided into small elements to eliminate the stress nonuniformity. The fatigue limit reliability is predicted by unifying the survival rates of the elements obtained by the stress-strength model according to the weakest link model. The method is applied to notched specimens of aluminum cast alloy JIS AC4B-T6 containing eutectic Si, Fe compounds and porosity. The fatigue strength reliability at 10^7 cycles, which corresponds to the fatigue limit reliability, is predicted. The fatigue limits of notch root radius $\rho = 2, 1, 0.3,$ and 0.1 mm are obtained by rotating-bending fatigue tests. It is shown that the fatigue limits predicted by the present method are in good agreement with the experimental ones.

Keywords: metal fatigue, fatigue limit reliability, notch effect, aluminum cast alloy, inhomogeneity

1. Introduction

Aluminum cast alloys are widely applied, for example, in motor vehicles, ships, aircraft, machines, and structures, owing to the high cast ability and high specific strength [1–3]. They can be improved so as to meet specific mechanical properties by tuning the casting method, the alloying elements, and the cooling and heat treatment conditions [4–6]. Generally, precipitation hardening, also called age-hardening, is used to strengthen the aluminum cast alloys, which brings the dense precipitate of particles such as eutectic Si. The precipitations form fine microstructures such as dendrites, which significantly improve the mechanical properties.

However, the resultant stress concentrations by the precipitations further to fatigue fracture unfortunately [7–9]. Moreover, the possibility of the fatigue fracture increases more and more if microstructural flaws such as porosity are created in the casting process [10–15]. Because the precipitate particles and the microstructural defects are unique, the fatigue strength of the aluminum cast alloys is obliged to treat statistically.

Statistical fatigue test methods [16, 17] are standardized to determine the reliability of the fatigue strength. However, because they require many fatigue tests, it is time-consuming to determine the fatigue strength reliability at 10^7 stress cycles. Moreover, because the weakest region which controls the fatigue strength of the specimen is not known, the present materials cannot be improved rationally. Hence, a faster, rational method for quantitatively and nondestructively predicting the effect of inhomogeneities on fatigue strength is necessary for safe and reliable machine designs and for economical and quick material developments.

Several methods for predicting the fatigue strength at 10^7 stress cycles, which are equivalent to the statistically determined fatigue limit of aluminum cast alloys, have been proposed [18–24]. Through a series of stress analyses and fatigue experiments, Murakami et al. [18–20] clarified the non-propagation limit of a fatigue crack initiated by a microstructural defect and proposed a simple formula for predicting the fatigue limit of a plain specimen containing defects [18–20]. The non-propagation limit of a fatigue crack initiated by microstructural defect is determined by the defect size and mechanical characteristics of the matrix near the defect. The maximum defect, which is often estimated by extreme statistics, is therefore assumed to be the origin of the fatigue fracture. Most of the methods are based on the assumption that fatigue fracture begins at the maximum defects, and they often do not consider the interference effects of inhomogeneities and the scatter of the hardness of the matrix [25]. Because aluminum cast alloys have much higher densities of inhomogeneities, it is presumed that the interference effect is not negligible and the maximum inhomogeneity is not in the severest mechanical state necessarily. Additionally, in the case of a notched specimen, the stress varies significantly. The most severe mechanical defect should be used for prediction, even if it is not maximal. Generally, the fatigue limit of a notched specimen of a homogeneous metal in which microstructural defect is not the origin of the fatigue fracture consists of the microcrack and macrocrack non-propagation limits [26–32]. This fact is widely used in predicting fatigue limit. However, since microstructural defects act as crack initiation sites, the fatigue limit of an inhomogeneous metal also cannot be predicted by these two types of crack non-propagation limits.

In this study, a quantitative method for predicting the fatigue limit reliability of a notched metal containing inhomogeneous particles is proposed. The present method is also based on the stress-strength model and is applied to notched specimens of an Al-Si-Cu alloy (JIS AC4B). The inhomogeneous particle in the alloy comprises eutectic Si and Fe compounds and porosity in the matrix. Rotating-bending fatigue tests are performed on the notched specimens of AC4B-T6 by changing notch root radius variously. The validity of the present method is examined by comparing its numerical prediction with experimental results.

2. Crack non-propagation limits for predicting fatigue limit of notched specimen

Generally, when fatigue tests are performed on a notched specimen by changing the notch root radius ρ for a given notch depth t , the typical relationship between the fatigue limit σ_w and ρ is as shown in **Figure 1**; here, σ_{w0} is the fatigue limit of the

Nomenclature	
t	notch depth
ρ	notch root radius
ρ_0	branch point
ρ_d	limit notch root radius
σ_w	fatigue limit of notched specimen
σ_{w0}	fatigue limit of plain specimen
σ_{w1}	microcrack non-propagation limit
σ_{w2}	long macrocrack non-propagation limit
σ_{wd}	small macrocrack non-propagation limit

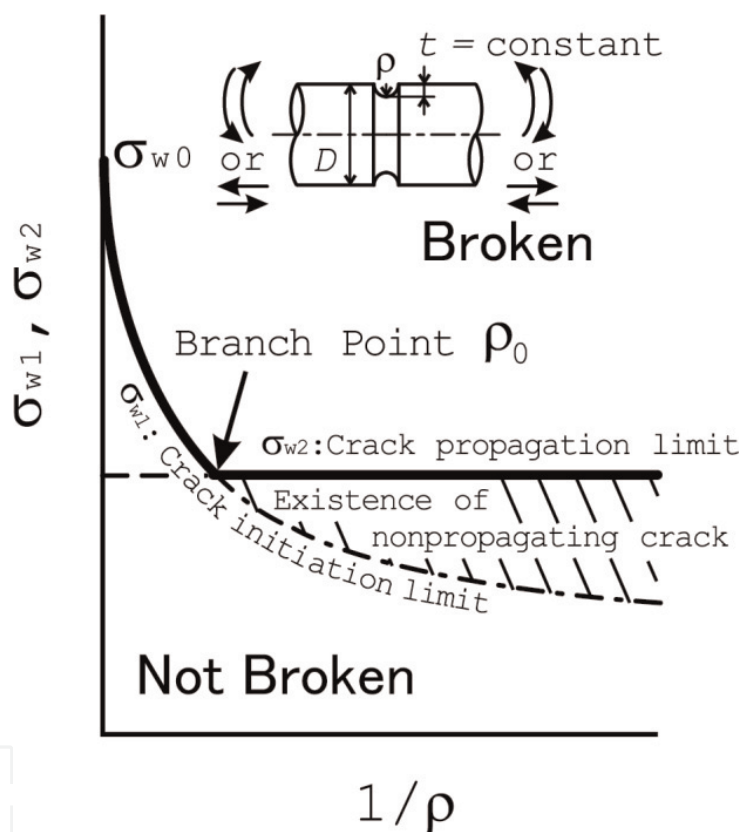


Figure 1. Schematic illustration of fatigue limit of a notched structure without defects.

plain specimen, σ_{w1} is the microcrack non-propagation limit, σ_{w2} is the macrocrack non-propagation limit, and ρ_0 is a material property known as the branch point, the critical value of which determines whether the non-propagating crack exists along the notch root [26, 27]. If the notch is sufficiently deep, ρ_0 is constant [27].

If $\rho > \rho_0$, σ_{w1} is the fatigue limit [33]. σ_{w1} can be predicted from the mechanical characteristics of the microstructure. Conversely, if $\rho \leq \rho_0$, σ_{w2} is the fatigue limit [33]. σ_{w2} is constant and independent of ρ . This means that the σ_{w2} is equal to the fatigue limit of the cracked specimen as $\rho \rightarrow 0$. That is, the notch can be assumed to be a crack and σ_{w2} can be predicted by the fracture mechanics.

In the case of metals containing microstructural defects, the non-propagation limit of the fatigue crack that originates from the microstructural defect may be the fatigue limit. Because the defect is categorized as a macrocrack, the low macrocrack

non-propagation limit is differentiated from σ_{w2} . The threshold stress intensity factor range ΔK_{th} determines whether the fatigue crack originating from the macrocrack is arrested. The value of ΔK_{th} is an indication of the dependency of the different crack lengths [20]. In this study, a crack for which ΔK_{th} is constant irrespective of its length, and which exhibits the small-scale yielding (SSY), is defined as a long macrocrack. Conversely, a crack for which ΔK_{th} is dependent on the length, and which exhibits the large-scale yielding (LSY), is defined as a small macrocrack [33, 34]. The three following types of crack non-propagation limits are introduced and defined to predict the fatigue limit of a notched specimen of aluminum cast alloy [35]:

σ_{w1} :	This is the non-propagation limit of a microcrack that is initiated by repeated irreversible plastic strains in a homogeneous notch stress field without microstructural and structural stress concentrations
σ_{wd} :	This is the non-propagation limit of a three-dimensional fatigue crack that originates from microstructural defects such as nonmetallic inclusions and pits in a homogeneous notch stress field without other microstructural and structural stress concentrations
σ_{w2} :	This is the non-propagation limit of structural long macrocracks such as deep notches with $\rho < \rho_0$

Figure 2 is a schematic illustration of the relationships between ρ and each of σ_{w1} , σ_{wd} , and σ_{w2} . Further, ρ_0 and ρ_d are, respectively, the branch point and limit notch root radius, which determines whether the fatigue limit is affected by the microstructural defects. σ_{w1} and σ_{wd} decrease as ρ decreases, whereas σ_{w2} attains a constant value and becomes independent of ρ . If $\rho \geq \rho_d$, σ_{wd} is equal to the fatigue limit σ_w . If $\rho_0 < \rho < \rho_d$, σ_{w1} is equal to σ_w . If $\rho \leq \rho_0$, σ_{w1} and σ_{wd} are cut off by σ_{w2} , and σ_{w2} is equal to σ_w .

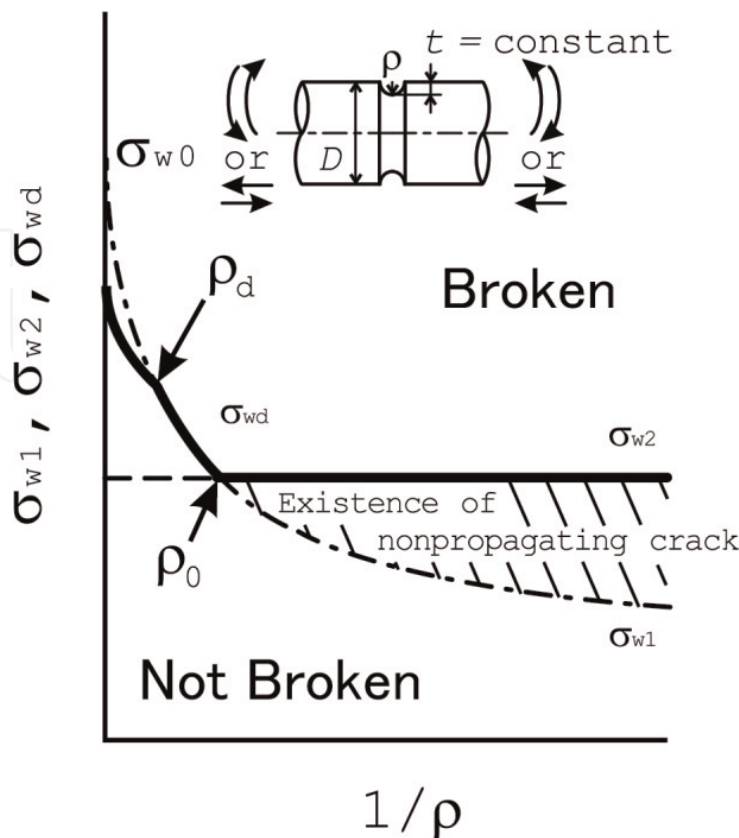


Figure 2. Schematic illustration of fatigue limit of a notched structure with defects.

Because the hardness is locally scattered and numerous defects are distributed through the material, the microcrack and defect that determine the fatigue fracture cannot be determined in advance. In this situation, the probabilities of the arrest of the microcrack and the fatigue crack originating from the defect are, respectively, determined by the statistical characteristics of the hardness and the statistical characteristics of the defect. That is, σ_{w1} and σ_{wd} are, respectively, described by probability distributions.

3. Method for predicting fatigue limit reliability of notched metal containing inhomogeneous particles

Nomenclature	
A_j	size of j th surface element
A_j^*	size of j th region where the relative first principal stress corresponds to $\sigma_{1,j}^*$
$A_{npc}, A_{npc R}, A_{npc P}$	region required for the non-propagation of fatigue crack
$\sqrt{area_p}$	size of surface defect
$\sqrt{area_{p1}}$	lower limit size of small surface crack
$\sqrt{area_R}$	size of internal defect
F, F_P, F_R	geometric correction factor
F_{σ_w}	fatigue limit reliability of notched specimen
$f_{H_{VM1}}, f_{H_{VM5}}, f_{H_{VMR}}, f_{H_{VMP}}$	H_{VM} distribution
f_{χ^2}	χ^2 distribution
g_P, g_R, g_S	limit hardness
γ_m	stress relaxation effect
H_V, H_{VM}	Vickers hardness
K_{In}, K_{IP}, K_{IR}	stress intensity factor
K_t	stress concentration factor
ΔK_w	threshold stress intensity factor range
ΔK_{wLL}	lower limit value of ΔK_w
ΔK_{wUL}	upper limit value of ΔK_w
$M_{S0}(\sqrt{area_{p0}})$	the number of surface cracks with $\sqrt{area_p} \geq \sqrt{area_{p0}}$ in a unit area
$M_{V0}(R_0)$	the number of particles with $R \geq R_0$ in a unit volume
M_d	types of inhomogeneous particles
\bar{N}_{V0}	the number of particles in a unit volume
n_S	the number of surface elements
n_V	the number of solid elements
P, P_R	indentation load
$P_V(R_0)$	existence probability of particles with $R \geq R_0$
R_c	limit size of small interior crack
S_{σ_w}	survival rate of notched specimen
$S_{\sigma_{w1}}$	survival rate of surface element with microcracks

$S_{\sigma_{wd}}, S_{\sigma_{wdl}}, S_{\sigma_{wds}}$	survival rate of solid element with microstructural defects
$s_{H_{VM}}^2$	population of H_{VM} distribution
V_j	size of j th solid element
λ, ν	material constant
$\mu_{H_{VM}}$	mean of H_{VM} distribution
$\sigma_1, \sigma_{1,j}$	first principal stress
$\sigma_1^*, \sigma_{1,j}^*$	relative first principal stress
$\sigma_{ym}(T_m, Z_m), \sigma_{zm}(T_m, Z_m)$	stress produced by the spherical particle in the infinite body under $\sigma_z = Z_m$ and $\sigma_x = \sigma_y = \sigma_z = T_m$
σ_m	mean stress
σ_n	stress amplitude
χ_{σ_1}	stress gradient of first principal stress

This section presents a method for predicting the fatigue limit reliability of a notched specimen with stress concentration factor K_t , notch depth t , and notch root radius ρ under zero mean stress. The control volume is actually divided into surface and solid elements so that the stresses applied to the elements can be assumed to be constant. The fatigue strengths of all the elements are then stochastically evaluated by the stress-strength model on the mesoscale. The fatigue limit reliability is also predicted by assembling the fatigue strengths using the weakest link model [25].

3.1 Stress relaxation effect of interference of inhomogeneous particles

Figure 3 is a schematic illustration of the analytical model of a metal containing inhomogeneous particles. The metal is approximated by a cubic lattice model to determine the stress relaxation effect of the interference of the particles [36].

3.1.1 Statistical characteristics of inhomogeneous particles

The probability of existence of such particles is given by the following equation [37]:

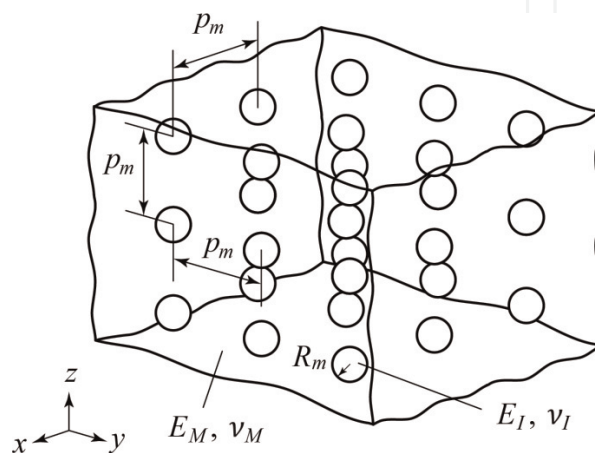


Figure 3.
Approximate model of metal with inhomogeneous particles.

$$P_V(R_0) = \exp \left\{ - \left(\frac{R_0}{\lambda} \right)^\nu \right\}. \quad (1)$$

Here, ν and λ are material constants, R_0 is the particle radius, and $P_V(R_0)$ is the probability of the existence of particles with radii greater than R_0 .

The total number of particles in a unit volume is denoted by \bar{N}_{V0} . The average number of particles with radii greater than R_0 in a unit volume, $M_{V0}(R_0)$, is given by the following equation [37]:

$$M_{V0}(R_0) = \bar{N}_{V0} \cdot P_V(R_0). \quad (2)$$

A particle cross-sectioned by the specimen surface is projected onto a plane perpendicular to the first principal stress. The projected area is then modified as shown in **Figure 4** by considering the mechanics. The modified area is denoted by $area_p$. The average number of cross-sectioned particles with areas larger than $\sqrt{area_{p0}}$ in a unit area, $M_{S0}(\sqrt{area_{p0}})$, is given by the following equation [12, 24]:

$$M_{S0}(\sqrt{area_{p0}}) = \lambda \bar{N}_{V0} \int_0^1 \frac{t}{\sqrt{1-t^2}} \left\{ \Gamma \left(1 + \frac{1}{\nu}, \left(\frac{\sqrt{area_{p0}}}{\lambda \theta^-} \right)^\nu \right) + \Gamma \left(1 + \frac{1}{\nu}, \left(\frac{\sqrt{area_{p0}}}{\lambda \theta^+} \right)^\nu \right) \right\} dt, \quad (3)$$

$$\theta^+ = \frac{\pi}{2} + 2\sqrt{1-t^2}, \quad (4)$$

$$\theta^- = \sin^{-1}t - t\sqrt{1-t^2}. \quad (5)$$

Here, Γ is a gamma function of the second kind.

3.1.2 Average radius and distance

The average particle radius is evaluated by the following equation:

$$R_m = \int_0^\infty R \frac{dP_V}{R} dR = \lambda \Gamma \left(1 + \frac{1}{\nu} \right). \quad (6)$$

If \bar{N}_{V0} particles are regularly arranged in a unit volume as shown in **Figure 3**, the average distance between the particles is evaluated by the following equation:

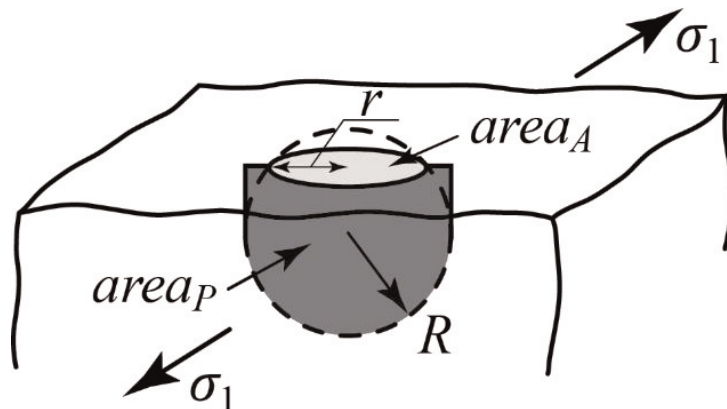


Figure 4.
 Spheroidal particle cut by surface.

$$p_m = \left(\frac{1}{\overline{N}_{V0}} \right)^{1/3} \quad (7)$$

3.1.3 Stress relaxation effect

Nisitani [38] proposed a method for approximately solving the interference problem of notches by superposing simple basic solutions to satisfy the equilibrium conditions at the stress concentration point.

When the uniform tensile stress at infinity, $\sigma_{z\infty} = 1$, is applied to an infinite body, it is supposed that a stress field composed of $\sigma_z = Z_m$ and $\sigma_x = \sigma_y = \sigma_z = T_m$ is formed around the particle. T_m and Z_m are set to satisfy the equilibrium condition at point $(0, 0, R_m)$. Because the stress acting on a single particle in the z -direction, $T_m + Z_m$, is composed of $\sigma_{z\infty} = 1$ and the stresses due to the other particles, the stress equilibrium condition in the z -direction is as follows:

$$T_m + Z_m = 1 + \sum_{\substack{(i,j,k) \neq (0,0,0) \\ i,j,k = -\infty}}^{\infty} \sum \sigma_{zm}(T_m, Z_m) \Big|_{\substack{x_{i,j,k} = -ip_m \\ y_{i,j,k} = -jp_m \\ z_{i,j,k} = R_m - kp_m}} \quad (8)$$

Here, $\sigma_{zm}(T_m, Z_m)$ is the stress in the z -direction at $(0, 0, R_m)$ produced by the spherical particle located at (ip_m, jp_m, kp_m) in the infinite body under $\sigma_z = Z_m$ and $\sigma_x = \sigma_y = \sigma_z = T_m$.

The stress equilibrium condition in the y -direction is also given by

$$T_m = \sum_{\substack{(i,j,k) \neq (0,0,0) \\ i,j,k = -\infty}}^{\infty} \sum \sigma_{ym}(T_m, Z_m) \Big|_{\substack{x_{i,j,k} = -ip_m \\ y_{i,j,k} = -jp_m \\ z_{i,j,k} = R_m - kp_m}} \quad (9)$$

Here, $\sigma_{ym}(T_m, Z_m)$ is the stress in the y -direction at $(0, 0, R_m)$ produced by the spherical particle located at (ip_m, jp_m, kp_m) in the infinite body under $\sigma_z = Z_m$ and $\sigma_x = \sigma_y = \sigma_z = T_m$.

T_m and Z_m are obtained by solving the simultaneous linear Eqs. (8) and (9). In this study, the stress relaxation effect γ_m of the interference of the particles is assumed to be

$$\gamma_m = T_m + Z_m. \quad (10)$$

3.1.4 Characteristics of elastic stress field near notch root

If the notch is sufficiently deep, a unique stress field determined by the maximum stress and ρ is formed near the notch root [27]. The first principal stress normalized by the maximum stress at the notch root is denoted by σ_1^* . **Figure 5** shows a contour map of $\sigma_1^* = [0.4, 1]$ near the notch root in a semi-infinite plate under tensile stress [35]. The value of σ_1^* is independent of the notch shape [27]. If the notch root is divided as shown in **Figure 5**, the length of the notch edge and size of j -th region in which the relative first principal stress is $\sigma_{1,j}^*$ are denoted by l_j^* and A_j^* ($j = 1, \dots$), respectively. The values of l_j^* and A_j^* are given in **Table 1** [35].

To predict the fatigue limit reliability, the control volume is set at the notch root and divided into surface and solid elements. The sizes of the solid and surface

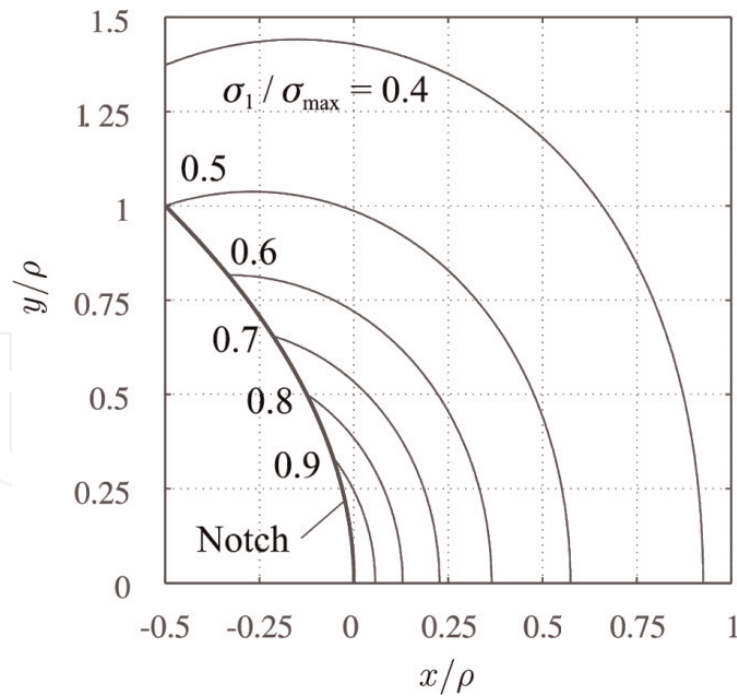


Figure 5.
 Contour map of relative first principal stress $\sigma_1^* = [0.4, 1]$ near the notch root.

j	1	2	3	4	5	6
$\sigma_{1,j}^*$	1–0.95	0.95–0.9	0.9–0.8	0.8–0.7	0.7–0.6	0.6–0.5
l_j^*/ρ	0.463	0.216	0.361	0.358	0.402	0.496
A_j^*/ρ	0.0083	0.0181	0.0703	0.144	0.296	0.657

Table 1.
 Area of isostress near the notch root.

elements are denoted by V_j and A_j ($j = 1, \dots$), respectively. In the case of a typical notch, as in the notched specimen, the control volume can be divided as shown in **Figure 5**. For example, when a circular bar with a circumferential notch is divided, V_j and A_j are approximated as follows [35]:

$$V_j \cong A_j^* \times (\text{average diameter of } j \text{ th region}) \times \pi, \quad (11)$$

$$A_j \cong l_j^* \times (\text{average diameter of } j \text{ th region}) \times \pi. \quad (12)$$

3.2 Fatigue survival rate of surface element containing microcracks

3.2.1 Statistical characteristics of Vickers hardness

The authors proposed a virtual small cell model for predicting the statistical characteristics of the Vickers hardness in a small region [25, 35]. If the population of the virtual small cells is described by an arbitrary distribution of the mean μ and variance s^2 , the statistical characteristics of the Vickers hardness can be described by the normal distribution of the mean μ and the variance s^2/n_c , based on the central limit theory, where n_c is the number of virtual small cells in the indentation area.

If m_1 Vickers hardness values are measured in this way using an indentation load P , their statistical characteristics are described by the following normal distribution [25, 35]:

$$f_{H_{VM1}}(H_{VM}) = \frac{1}{\sqrt{2\pi s_{H_{VM1}}^2}} \exp \left\{ -\frac{(H_{VM} - \mu_{H_{VM1}})^2}{2s_{H_{VM1}}^2} \right\}. \quad (13)$$

Here, H_{VM} is the Vickers hardness of the matrix that does not contain microstructural defects, $\mu_{H_{VM1}}$ is the sample mean, and $s_{H_{VM1}}^2$ is the sample variance.

Based on the central limit theorem, the relationship between the sample mean $\mu_{H_{VM1}}$ and the population mean $\mu_{H_{VM0}}$ is $\mu_{H_{VM1}} = \mu_{H_{VM0}}$. Further, the relationship between the sample variance $s_{H_{VM1}}^2$ and the population variance $s_{H_{VM0}}^2$ is described by the χ^2 distribution with the freedom degree of $n = m_1 - 1$ [25, 35]:

$$f_{\chi^2}(\chi^2) = \frac{1}{2\Gamma(n/2)} \left(\frac{\chi^2}{2}\right)^{\frac{n}{2}-1} \exp\left(-\frac{\chi^2}{2}\right) \quad (14)$$

$$\Gamma(t) = \int_0^{\infty} x^{t-1} e^{-x} dx, \chi^2 = m_1 \frac{s_{H_{VM1}}^2}{s_{H_{VM0}}^2} \quad (15)$$

3.2.2 Fatigue survival rate of surface element containing microcracks

The microcrack non-propagation limit σ_{w0} is determined by the average characteristics of the material properties around the microcrack. σ_{w0} can be empirically predicted by the following equations [20, 26]:

$$\sigma_{w0}|_{\sigma_m=0} = 1.6 H_{VM}, \quad (16)$$

$$\sigma_{w1}|_{\sigma_m=0} = \frac{\sigma_{w0}|_{\sigma_m=0}}{K_t \sqrt{1 + 4.5\varepsilon_0|_{\sigma_m=0}/\rho}} = f(H_{VM}, \rho, \sigma_m = 0, K_t). \quad (17)$$

(σ_{w0} , σ_{w1} , and σ_m are in MPa, H_{VM} is in kgf/mm², and ρ and ε_0 are in mm.)

If the stress relaxation effect γ_m is considered, $\gamma_m \sigma_{1,j}$ is applied to j -th surface element. Because fatigue fracture occurs when $\gamma_m \sigma_{1,j}/K_t$ is greater than σ_{w1} , the limit hardness $g_S(\sigma_{1,j})$ that determines the occurrence is given by the following equation:

$$g_S = f^{-1}(H_{VM}, \rho, \sigma_m = 0, K_t)|_{\sigma_{w1}=\gamma_m \sigma_{1,j}/K_t}. \quad (18)$$

Here, f^{-1} is a function obtained by solving Eq. (18) on H_{VM} .

It is supposed that $A_{npc S}$ exhibits the microcrack non-propagation limit characteristics in Eqs. (16) and (17). If H_{VM} of the matrix is greater than g_S in $A_{npc S}$, fatigue fracture will not occur in $A_{npc S}$. Therefore, the probability $S_{\sigma_{w1}0,j}$ that fatigue fracture does not occur in $A_{npc S}$ below $\sigma_{1,j}$ is given by [25, 35]

$$S_{\sigma_{w1}0,j} = \int_{g_S}^{\infty} f_{H_{VM}S}(h_{vm}) dh_{vm}. \quad (19)$$

Here, $f_{H_{VM}S}$ is the normal distribution of $\mu_{H_{VM}S}$ and $s_{H_{VM}S}^2$.

The fatigue survival rate $S_{\sigma_{w1},j}$ of j th surface element containing microcracks is given by the following equation [25, 35]:

$$S_{\sigma_{w1},j} = \int_0^{\infty} f_{\chi^2} \cdot (S_{\sigma_{w1}0,j})^{\frac{A_j}{A_{npc S}}} d\chi^2. \quad (20)$$

If fatigue fracture does not occur in all the surface elements, the notched specimen would not be broken by the microcrack. Therefore, the fatigue survival rate of a surface element containing microcracks, $S_{\sigma_{w1}}$, is obtained by multiplying the fatigue survival rates of all the surface elements as follows [25, 35]:

$$S_{\sigma_{w1}} = \prod_{j=1}^{n_S} S_{\sigma_{w1},j}. \quad (21)$$

Here, n_S is the number of surface elements.

3.3 Fatigue survival rate of surface element containing microstructural defects

The authors [25] proposed a method for predicting the reliability of the small macrocrack non-propagation limit for a nonzero stress gradient using the “statistical hardness characteristics of a matrix under small indentation loads” and the “statistical hardness characteristics required for non-propagation of fatigue cracks originating from microstructural defects in a material” [25]. The stress relaxation effect was introduced into the method to make it applicable to a metal containing dense inhomogeneous particles.

σ_{wd} is divided into two crack non-propagation limits, namely, the non-propagation limit σ_{wdI} of the small crack originating from the interior defect and the non-propagation limit σ_{wdS} of the small crack originating from the surface defect.

3.3.1 Fatigue survival rate of solid element containing interior microstructural defects

Because the fatigue crack that originates from a defect propagates on the plane perpendicular to the first principal radial stress, a spherical particle of radius R is projected onto this plane and assumed to be a penny-shaped crack. If the projected area is denoted by $area_R$, its square root is related to R as follows:

$$\sqrt{area_R} = \sqrt{\pi}R. \quad (22)$$

The stress intensity factor K_{IR} of the small interior crack is given by [20, 35]

$$K_{IR} = 0.5 F_R \gamma_m \sigma_{1,j} \sqrt{\pi \sqrt{area_R}}, \quad (23)$$

$$F_R = \frac{4}{\pi^{5/4}} \left\{ 1 - \left(\frac{2}{\sqrt{\pi}} - \frac{4}{3\pi} \right) \frac{\sqrt{area_R}}{\rho} \right\}. \quad (24)$$

Moreover, the threshold stress intensity factor range ΔK_w of the small surface defect of size $\sqrt{area_P}$ in the metal with Vickers hardness H_{VM} is given by the following equation [33, 34]:

$$\Delta K_w|_{\sigma_m=0} = \frac{2\alpha\beta\sqrt{area_P}^{1/3}}{\ln(2\beta/H_{VM} + 1)}, \quad (25)$$

$\alpha = 3.3 \times 10^{-3}$ and $\beta = 120$.

(ΔK_w is in $\text{MPa}\sqrt{\text{m}}$, H_{VM} is in kgf/mm^2 , and $\sqrt{area_P}$ is in μm).

The limit hardness that determines whether the fatigue crack originating from the interior microstructural crack is arrested, $g_R(\sigma_{1,j}, \sqrt{area_R})$, is given based on the relationship $\sqrt{area_R} = 1.7 \sqrt{area_P}$ by the following equation [25, 35]:

$$g_R = 240 / \left\{ \exp \left(\frac{1.56 \times 240}{F_R \gamma_m \sigma_{1,j} \sqrt{area_R}^{1/6}} \right) - 1 \right\} \quad (26)$$

($\sigma_{1,j}$ is in MPa, g_R is in kgf/mm², and $\sqrt{area_R}$ is in μm .)

The relationship between $\mu_{H_{VMR}}$ and $\mu_{H_{VM0}}$ can be expressed as follows [25, 35]:

$$\mu_{H_{VMR}} = \mu_{H_{VM0}} = \mu_{H_{VM1}}. \quad (27)$$

Moreover, the relationship between $s_{H_{VMR}}^2$ and $s_{H_{VM0}}^2$ can be expressed as follows [25, 35]:

$$A_{npc R} \cdot s_{H_{VMR}}^2 = A_{H_{VM0}} \cdot s_{H_{VM0}}^2. \quad (28)$$

Here, $A_{H_{VM0}} = P / \mu_{H_{VM0}}$, $A_{npc R} = P_R / g_R$, and P_R are the loads used to create the indentation for obtaining the Vickers hardness g_R and the indentation area $A_{npc R}$.

The fatigue survival rate of j -th solid element containing interior defects, $S_{\sigma_{wdl},j}^{(m)}$, is given by the following equation [25, 35]:

$$S_{\sigma_{wdl},j}^{(m)} = \int_0^\infty f \chi^2 \exp \left\{ - \int_\infty^{R_c} \left(\int_0^{g_R} p_{dI}^{(m)} \frac{dM_{V,j}^{(m)}}{dR} f_{H_{VMR}} dh_{vm} \right) dR \right\} d\chi^2. \quad (29)$$

If the fatigue fracture does not occur in all the solid elements, the notched specimen would not be broken by the small interior defect. Therefore, the fatigue survival rate $S_{\sigma_{wdl}}^{(m)}$ of a solid element containing interior microstructural defects is obtained by multiplying the fatigue survival rates of all the solid elements as follows [25, 35]:

$$S_{\sigma_{wdl}}^{(m)} = \prod_{j=1}^{n_V} S_{\sigma_{wdl},j}^{(m)}. \quad (30)$$

Here, n_V is the number of solid elements.

3.3.2 Fatigue survival rate of surface element containing surface microstructural cracks

The stress intensity factor K_{IP} of a small surface crack of size $\sqrt{area_P}$ is given by the following equation [20, 35]:

$$K_{IP} = 0.65 F_R \gamma_m \sigma_{1,j} \sqrt{\pi \sqrt{area_P}}, \quad (31)$$

$$F_P = 0.968 - 1.021 \frac{\sqrt{area_P}}{\rho}. \quad (32)$$

Further, the limit hardness $g_P(\sigma_{1,j}, \sqrt{area_P})$ that determines whether the small surface crack is arrested is given by the following equation [25, 35]:

$$g_P = 240 / \left\{ \exp \left(\frac{1.43 \times 240}{F_R \gamma_m \sigma_{1,j} \sqrt{area_P}^{1/6}} \right) - 1 \right\}. \quad (33)$$

($\sigma_{1,j}$ is in MPa, g_P is in kgf/mm², and $\sqrt{area_P}$ is in μm .)

The fatigue survival rate of j -th surface element containing surface microstructural cracks, $S_{\sigma_{wdS},j}^{(m)}$, is given by

$$S_{\sigma_{wds},j}^{(m)} = \int_0^\infty f \chi^2 \exp \left\{ - \int_0^{\sqrt{area_Pc}} \left(\int_0^{g_P} p_{dS}^{(m)} \frac{dM_{S,j}^{(m)}}{d\sqrt{area_P}} f_{H_{VM}P} dh_{vm} \right) d\sqrt{area_P} \right\} d\chi^2 \quad (34)$$

The fatigue survival rate $S_{\sigma_{wds}}^{(m)}$ of a surface element containing surface microstructural cracks is obtained by multiplying the fatigue survival rates of all the surface elements as follows [25, 35]:

$$S_{\sigma_{wds}}^{(m)} = \prod_{j=1}^{n_S} S_{\sigma_{wds},j}^{(m)} \quad (35)$$

3.3.3 Fatigue survival rate of element with microstructural defects

The fatigue survival rate $S_{\sigma_{wd}}^{(m)}$ of an element containing microstructural defects is obtained by multiplying $S_{\sigma_{wdl}}^{(m)}$ and $S_{\sigma_{wds}}^{(m)}$ as follows [25, 35]:

$$S_{\sigma_{wd}}^{(m)} = S_{\sigma_{wdl}}^{(m)} \times S_{\sigma_{wds}}^{(m)} \quad (36)$$

Because the material contains M_d types of inhomogeneous particles, the fatigue survival rate $S_{\sigma_{wd}}$ is given by the following equation:

$$S_{\sigma_{wd}} = \prod_{m=1}^{M_d} S_{\sigma_{wd}}^{(m)} \quad (37)$$

3.4 Prediction of long macrocrack non-propagation limit σ_{w2}

σ_{w2} of the notched specimen with $\rho \leq \rho_0$ is equal to the fatigue limit of the cracked specimen obtained by $\rho \rightarrow 0$. ΔK_{wUL} is the upper limit of ΔK_w and is constant regardless of the crack length. $\sigma_{w2}|_{\sigma_m=0}$ can be obtained as follows [35]:

$$\sigma_{w2}|_{\sigma_m=0} = \frac{\Delta K_{wUL}|_{\sigma_m=0}}{2F\sqrt{\pi t}} \quad (38)$$

3.5 Prediction of fatigue limit reliability

The probability that fatigue fracture is caused by microcracks or microstructural defects is obtained by the complementary event defined by the product of $S_{\sigma_{w1}}$ and $S_{\sigma_{wd}}$. Because the fatigue limit of a notched specimen, σ_w cannot be lower than σ_{w2} , and its fatigue limit reliability F_{σ_w} is obtained as follows [35]:

$$F_{\sigma_w} = \begin{cases} 0 & (\sigma_w \leq \sigma_{w2}) \\ 1 - S_{\sigma_{w1}} \times S_{\sigma_{wd}} & (\sigma_w > \sigma_{w2}) \end{cases} \quad (39)$$

4. Fatigue experiment

4.1 Material, shape of specimen, and experimental procedure

The material used for the experiment was Al-Si-Cu alloy (JIS AC4B). The age-hardened aluminum cast alloy is identified as AC4B-T6. Table 2 shows its mechanical properties.

E	$\sigma_{0.2}$	σ_B	δ	H_V	H_{VM}
				9.8 N, 30 sec	29.4 mN, 30 sec
74	292	349	1.5	152	92
E : Young's modulus (GPa)				$\sigma_{0.2}$: 0.2% proof stress (MPa)	
σ_B : ultimate tensile strength (MPa)				δ : elongation (%)	
H_V : Vickers hardness of matrix with inhomogeneous particles (kgf/mm ²)					
H_{VM} : Vickers hardness of matrix without inhomogeneous particles (kgf/mm ²)					

Table 2.
Mechanical properties.

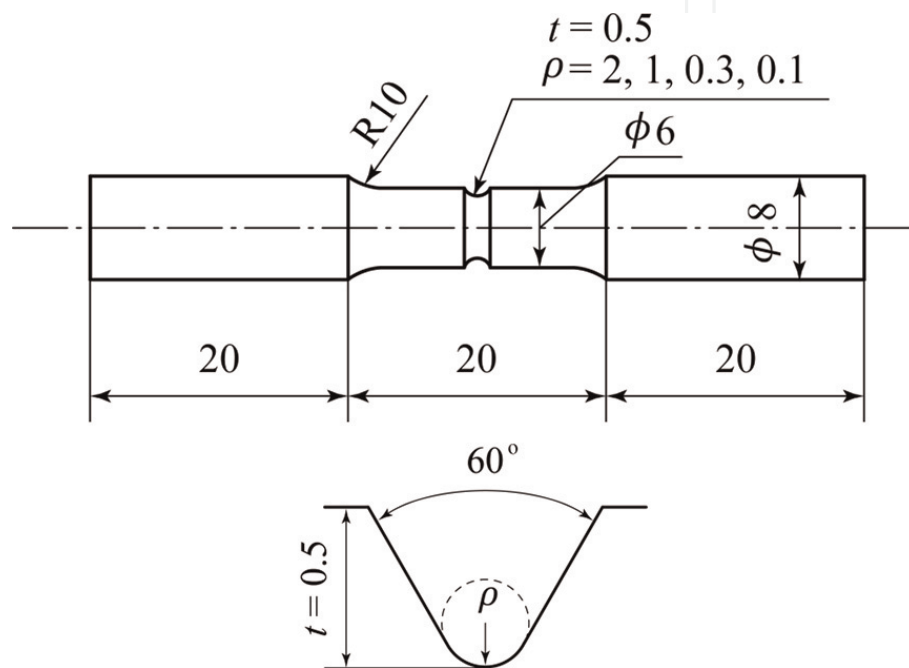


Figure 6.
Specimen configuration.

Figure 6 shows the configurations of the specimens. The notch depth t and opening angle θ were set at 0.5 mm and 60° , respectively. The notch root radii ρ were set at 2, 1, 0.3, and 0.1 mm, respectively. All the specimens were machined; polished with fine emery paper, alumina ($3\ \mu\text{m}$), and diamond paste ($1\ \mu\text{m}$); and also chemically polished. Rotating-bending fatigue tests were carried out according to JIS Z2274 and the earlier studies [27–31] under stress amplitude $\sigma_a = 60\text{--}110\ \text{MPa}$ and frequency $f = 50\ \text{Hz}$. An Ono-type rotating-bending fatigue machine of a capacity 15 Nm was used for the tests. The nominal stress σ_n used for the analyses of the experimental results was the stress at the minimum cross section, where the diameter d was 5 mm. The fatigue life N_f was defined as the total number of stress cycles to failure.

4.2 Experimental results

Figure 7 shows S - N curves obtained from the results of the tests. **Figure 8** shows optical micrographs of a specimen when $\rho = 0.1\ \text{mm}$ for $\sigma_w = 90\ \text{MPa}$. Fatigue limit $\sigma_w = 105$ when $\rho = 2\ \text{mm}$. $\sigma_w = 95$ when $\rho = 1$ and $0.3\ \text{mm}$. $\sigma_w = 90$ when $\rho = 0.1\ \text{mm}$. Since the non-propagating macrocrack was not observed at the fatigue

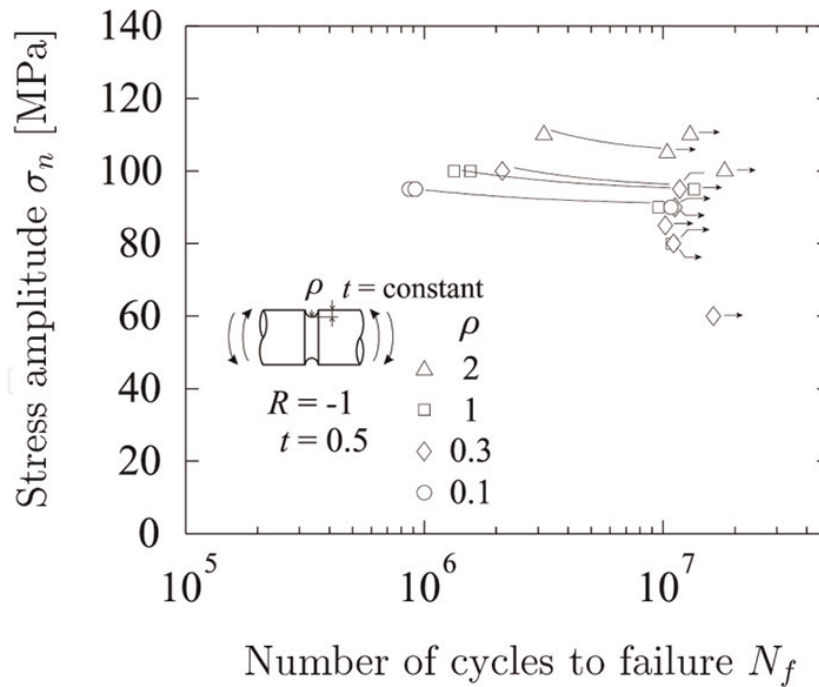


Figure 7.
S - N curve.

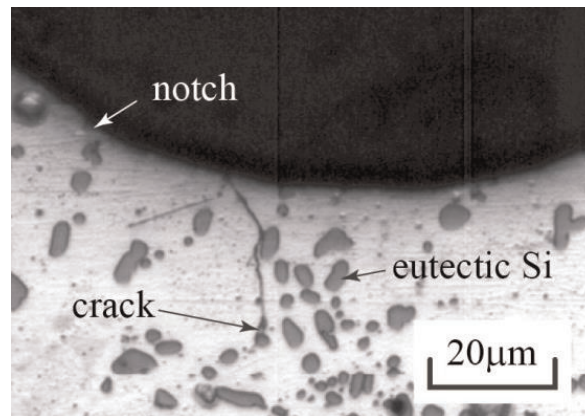


Figure 8.
Optical micrograph of non-propagating crack under notch root.

limit when $\rho = 1$ and 2 mm, it can be said that the microcrack non-propagating limit σ_{w1} or the small macrocrack non-propagating limit σ_{wd} appears as the fatigue limit. When $\rho = 0.1$ mm for $\sigma_w = 90$ MPa and $\rho = 0.3$ mm for $\sigma_w = 95$ MPa, the non-propagating macrocracks were observed along the notch root. Therefore, the long macrocrack non-propagating limit $\sigma_{w2} = 90$ MPa.

5. Examination of validity of prediction method

5.1 Notch sensitivity to crack initiation limit in age-hardened aluminum alloy

Figure 9 shows the relationship between $K_t \sigma_{w1} / \sigma_{w0}$ and ρ using early fatigue data of previous studies [28–30]. ϵ_0 values of the curves are shown in Figure 10. When ϵ_0 values were approximated with the lines by the least squares method, the following equation was obtained:

$$\begin{aligned} \varepsilon_0|_{\sigma_m=0} &= 5.0 \times 10^{-4} H_B - 0.0164, \\ \rho &\geq 0.5, 97 \leq H_B \leq 207. \end{aligned} \tag{40}$$

(ε_0 and ρ are in mm, and H_B is in kgf/mm^2 .)

Once σ_{w1} has been predicted, H_{VM} can be used instead of H_B .

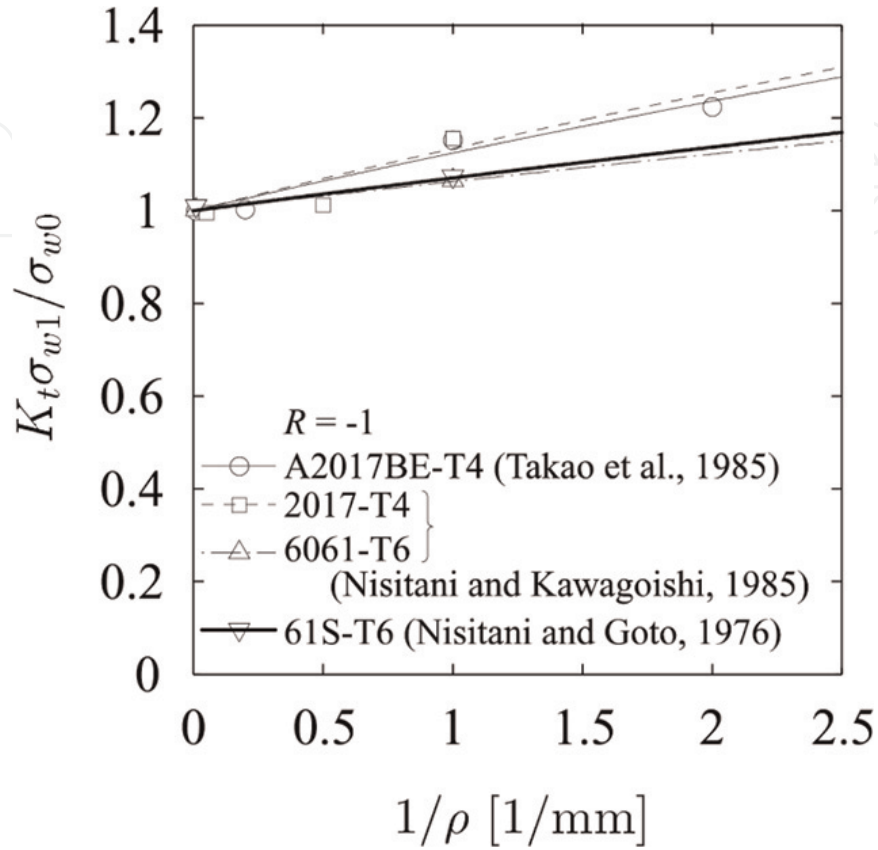


Figure 9.
Relation between $K_t \sigma_{w1} / \sigma_{w0}$ and $1/\rho$.

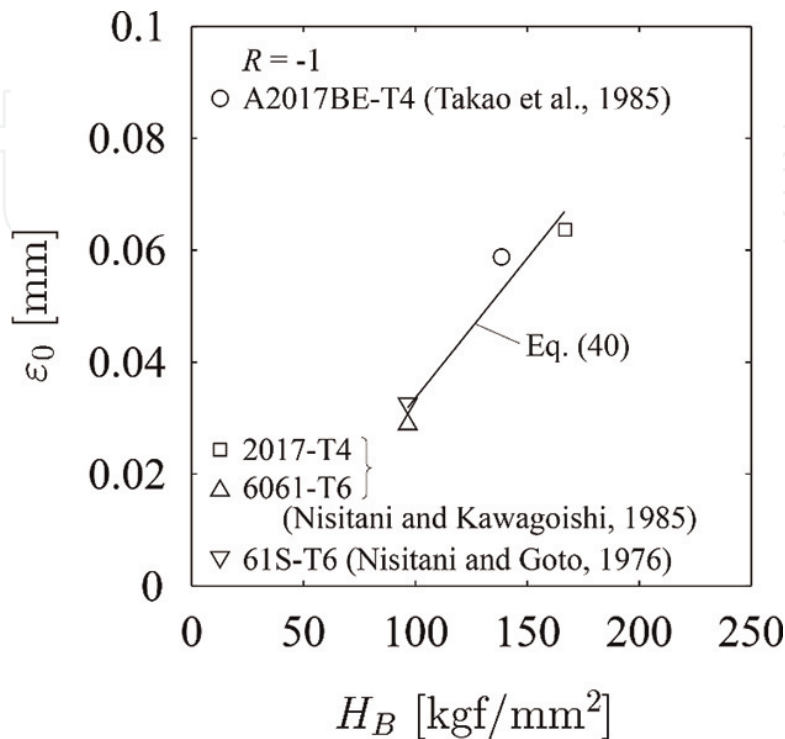


Figure 10.
Relation between ε_0 and H_B .

5.2 ΔK_{wUL} of age-hardened aluminum alloy

Figure 11 shows the values of ΔK_{wUL} obtained from the early fatigue data of σ_{w2} for different Al-Si-X alloys, where X is a transition element [28, 29, 31]. An approximation of ΔK_{wUL} obtained from the lines by the least squares method was used to derive the following equation:

$$\Delta K_{wUL}|_{\sigma_m=0} = \Delta K_{wLL} + 0.03 H_B, \quad (41)$$

$$40 \leq H_B \leq 100.$$

(ΔK_{wUL} and ΔK_{wLL} are in $\text{MPa}\sqrt{\text{m}}$, and H_B is in kgf/mm^2 .)

Here, ΔK_{wLL} is the lower limit of ΔK_w and $\Delta K_{wLL} = 0.5 \text{ MPa}\sqrt{\text{m}}$ for the Al-Si-X alloys.

5.3 Evaluation of statistical characteristics of inhomogeneous particles

The present aluminum cast alloy AC4B-T6 contains three main types of inhomogeneous particles, namely, eutectic Si and Fe compounds and porosity. Surrounding an irregular cross section with a smooth convex curve as shown in **Figure 12**, the area is defined as $area_A$. The values of r are obtained from $area_A$ by the following equation [12, 37]:

$$r = \frac{\sqrt{area_A}}{\sqrt{\pi}}. \quad (42)$$

Figure 13 shows the measured M_{A0} values of eutectic Si and Fe compounds and porosity. The relationship between M_{V0} and M_{A0} is as follows [12, 37]:

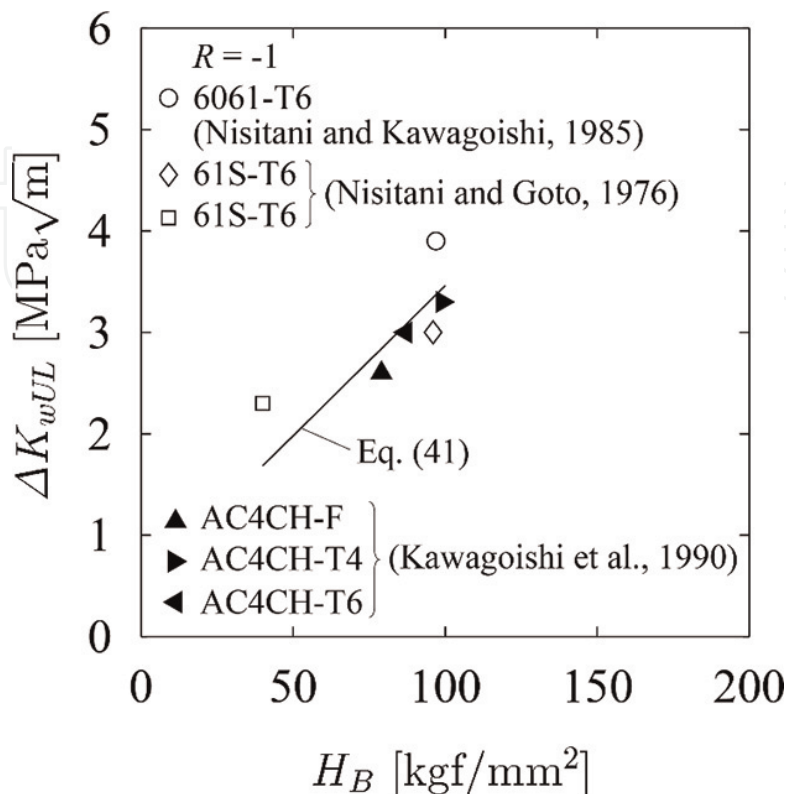


Figure 11.
 Relation between ΔK_{wUL} and H_B .

$$M_{A0}(r_0) = 2 \int_{\infty}^{r_0} \sqrt{R^2 - r^2} \frac{dM_{V0}}{dR} dR. \quad (43)$$

Here, $M_{A0}(r_0)$ is the number of cross-sectional particles in a unit area for which $r \geq r_0$ on a unit area. Considering the assumption that $M_{V0}(R_0)$ is given by Eqs. (1) and (2), the asymptotic characteristics of Eq. (42) are expressed by the following equation [12, 37]:

$$M_{A0}(r_0) \cong \sqrt{\frac{2\pi}{\nu}} \lambda \left(\frac{r_0}{\lambda}\right)^{1-\frac{\nu}{2}} \bar{N}_{V0} \exp\left\{-\left(\frac{r_0}{\lambda}\right)^\nu\right\}. \quad (44)$$

The line of Eq. (44) is drawn to best fit the M_{A0} values obtained by Eq. (43) to determine the values of \bar{N}_{V0} , ν , and λ .

Figure 14 shows the values of M_{V0} for porosity, Fe compounds, and eutectic Si. **Figure 15** shows the values of M_{S0} for the porosity, Fe compounds, and eutectic Si.

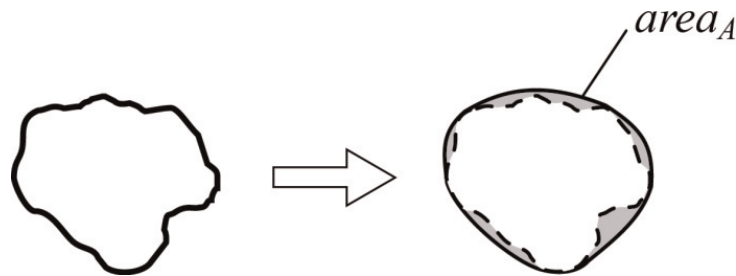


Figure 12.
Definition of $area_A$.

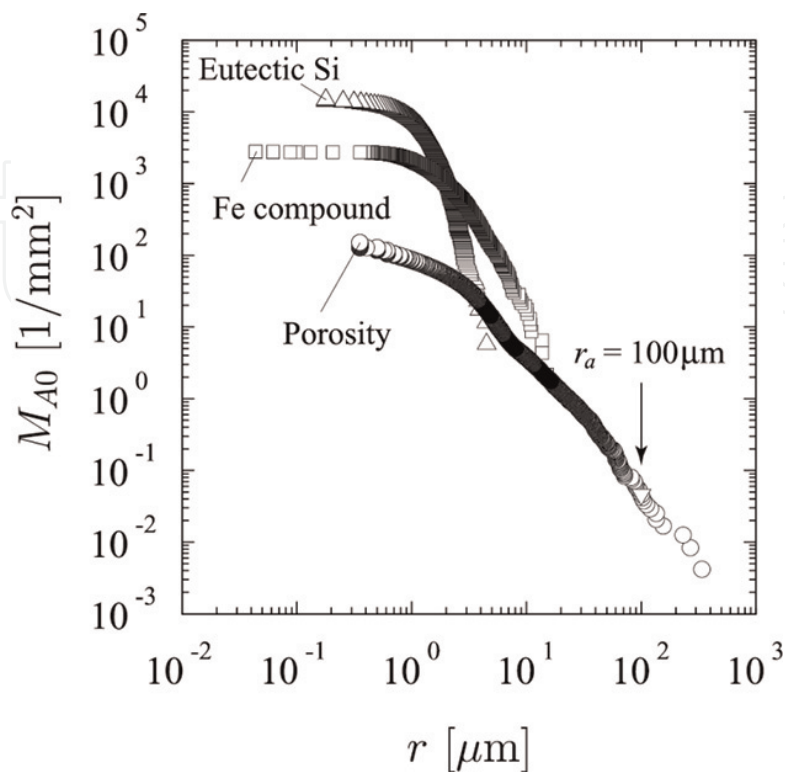


Figure 13.
 M_{A0} of porosity and eutectic Si and Fe compounds.

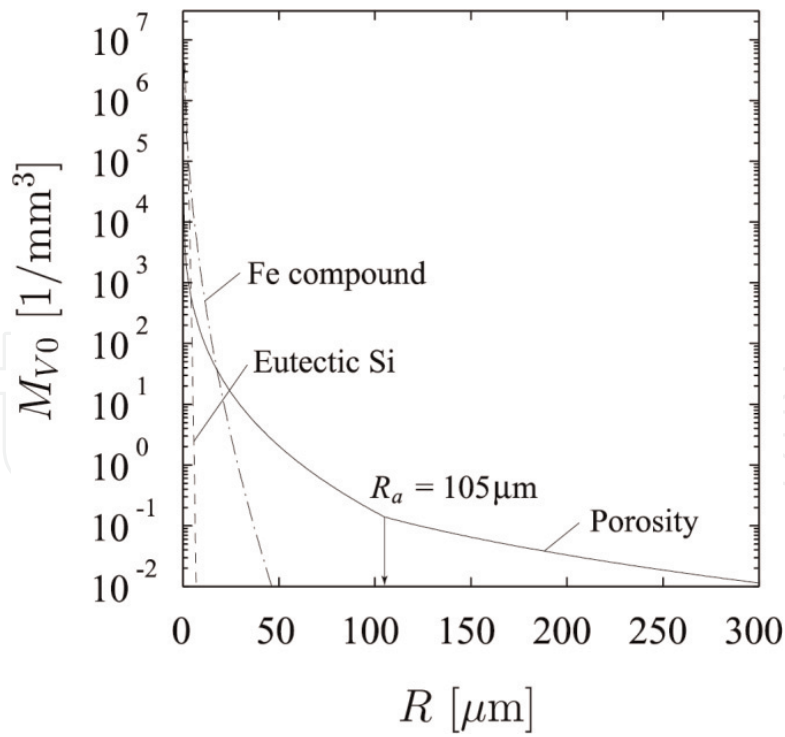


Figure 14.
 Relation between M_{V0} and R .

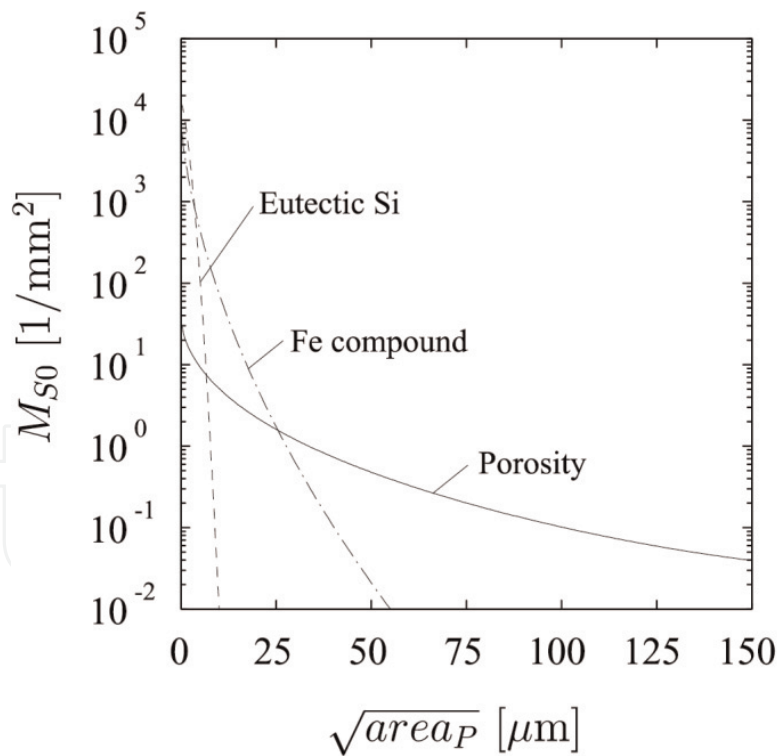


Figure 15.
 Relation between M_{S0} and $\sqrt{\text{area}_P}$.

5.4 Evaluation of statistical characteristics of Vickers hardness of matrix without inhomogeneous particles

In this study, the Vickers hardness was measured at the position of 2.5–3.0 mm from the center on the circular cross section obtained by cutting the specimen grip under indentation load $P = 29.4$ mN in consideration with the stress distribution at

the notch root. **Figure 16** shows the results plotted on a normal probability paper. The sample mean $\mu_{H_{VM1}}$ and sample variance $s_{H_{VM1}}^2$ were 91.8 kgf/mm² and 486.0 (kgf/mm²)², respectively.

5.5 Evaluation of γ_m value

Because the values of R_m/p_m for the eutectic Si were much greater than those of the Fe compounds and porosity, as shown in **Table 3**, γ_m was calculated using only the eutectic Si. The eutectic Si was assumed to be a rigid body [7], and the following values were used for the calculation: $E_M = 68$ GPa, $E_I = 105$ GPa, and $\nu_M = \nu_I = 0.3$ [35]. Using $R_m/p_m = 0.192$, γ_m was determined to be 1.055.

5.6 Evaluation of $A_{npc S}$, $A_{npc R}$, and $A_{npc P}$ values

5.6.1 Evaluation of $A_{npc S}$ value

Because a microcrack often grows radially, it is approximated by the semielliptical crack shown in **Figure 17**.

$A_{npc S}$ in Eq. (20) can also be roughly evaluated. The approximation of the microcrack by the semielliptical macrocrack is such that the crack non-propagation

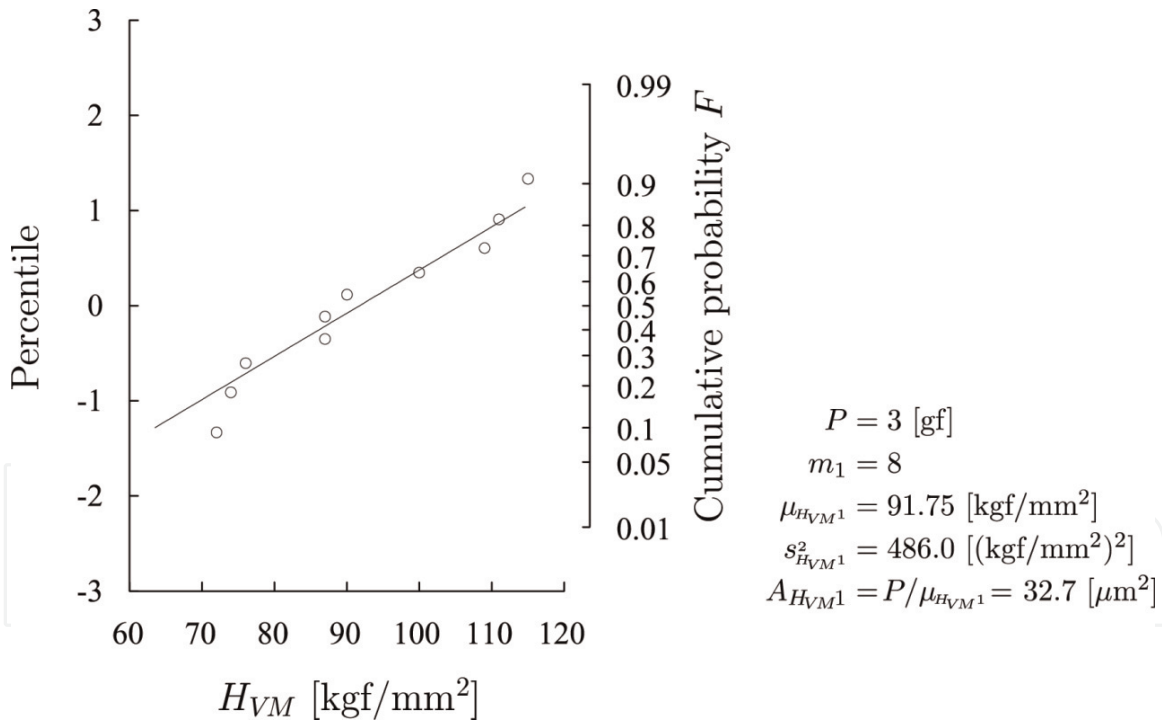


Figure 16. Evaluation of Vickers hardness of matrix from normal probability paper.

Inhomogeneous particle	\bar{N}_{V0} [1/mm ³]	ν	λ [μ m]	R_m [μ m]	p_m [μ m]
Eutectic Si	8.73×10^6	1.6	1.04	0.932	4.86
Fe compound	2.20×10^7	0.5	0.10	0.200	3.57
Porosity	($R \geq 105\mu$ m)	1.20×10^2	0.3	0.180	21.5
	($R < 105\mu$ m)	1.00×10^5	0.3	0.0180	

Table 3. Parameters of particle size distribution.

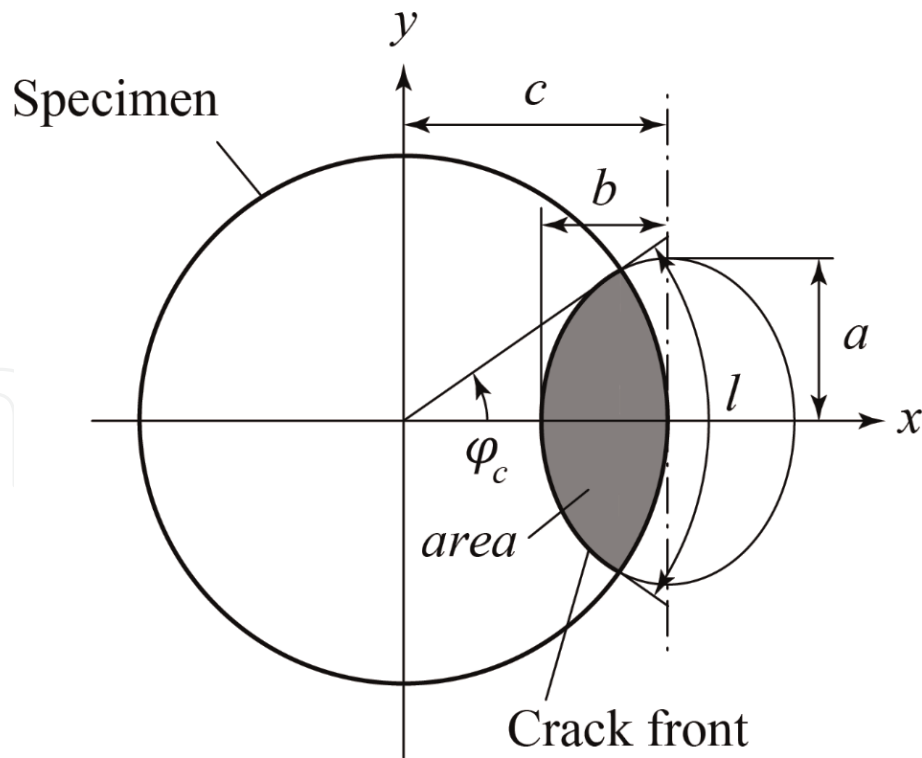


Figure 17.
 Schematic illustration of the microcrack.

limits are equal. If the macrocrack is located near the notch root of radius ρ and it is sufficiently small, its non-propagation limit σ_{wds} is given by the following equation:

$$\sigma_{wds} = \frac{1.43(H_{VM} + 120)}{F_P \sqrt{area_P}^{1/6}}, \quad (45)$$

$$F_P = 0.968 - 1.021 \times 10^{-3} \frac{\sqrt{area_P}}{\rho}. \quad (46)$$

(σ_{wds} is in MPa, H_{VM} is in kgf/mm^2 , $\sqrt{area_P}$ is in μm , and ρ is in mm.)

Conversely, when the macrocrack is sufficiently large, ΔK_w is greater than ΔK_{wUL} . The macrocrack is thus treated as being large, and its non-propagation limit is categorized as σ_{w2} , which is given by the following equation:

$$\sigma_{w2} = \frac{13.0(H_{VM} + 16.7)}{F_P \sqrt{area_P}^{1/2}}. \quad (47)$$

(σ_{w2} is in MPa, H_{VM} is in kgf/mm^2 , and $\sqrt{area_P}$ in μm .)

F_P is approximated to be 1. Because the average Vickers hardness of the matrix of the present AC4B-T6 is about $91.8 \text{ kgf}/\text{mm}^2$, the microcrack non-propagation limit σ_{w0} was estimated to be 160 MPa using Eq. (17). The non-propagating crack length of the present AC4B-T6 for $\rho = 20 \text{ mm}$ was about $60 \mu\text{m}$ when $\sigma_n = 120 \text{ MPa}$. From these experimental results, the l_{npc0} of the present study was assumed to be $70 \mu\text{m}$.

l_{npc} was set to achieve $b/l = 0.4$. Using $c = 2.5 \text{ mm}$, $l_{npc0} = 70 \mu\text{m}$ is equivalent to $\sqrt{area_{npc0}}$ of $39.2 \mu\text{m}$. **Figure 18** shows the relationship between l_{npc} and $1/\rho$.

5.6.2 Evaluation of A_{npcR} and A_{npcP} values

A_{npcR} is a function of P_R and g_R ; A_{npcP} is a function of P_P and g_P . Because g_R and g_P can be calculated using Eqs. (26) and (33), respectively, only P_R and P_P need to

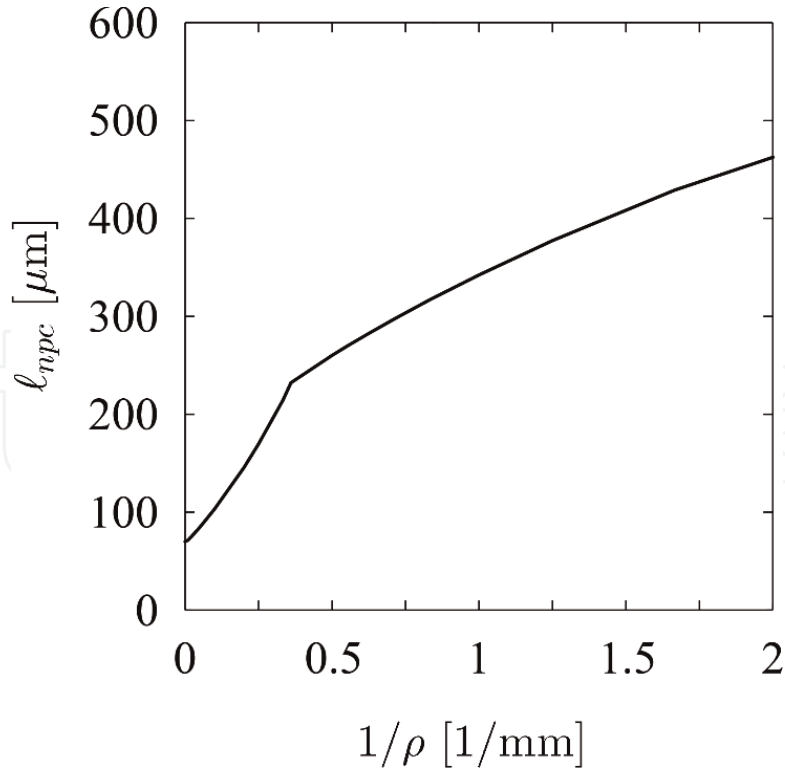


Figure 18.
Relation between l_{npc} and $1/\rho$.

be further examined. In this study, it is assumed that $P_P = 0.3$ kgf. Considering the difficulty in evaluating P_R , it is also assumed that $P_R = P_P$.

5.7 Comparison and examination of predicted and experimental results

The fatigue limit reliability of the notched specimen shown in **Figure 6** was predicted by the present method. The region in which the first principal stress is within the range of $\sigma_1^* = \sigma_1/\sigma_{max} = [0.95, 1]$ at the center of the specimen was adopted as the control volume. In this case, the region was ring-like.

When $H_B = 152$ kgf/mm² is used, the $\Delta K_{wUL} = 5.06$ MPa \sqrt{m} is predicted from Eq. (41). Because the value of ξ for the present specimen is 0.167 (i.e., using $d = 5$ mm and $t = 0.5$ mm, as in Section 4.1), F is 0.754 [39]. In this case, the predicted value of σ_{w2} is 84.7 MPa. Considering that the experimentally determined value of σ_{w2} is 90 MPa, the prediction is confirmed to be good.

Figure 19 shows the fatigue limit reliability F_{σ_w} . The thick solid line represents the case of $\rho = 2$ mm, whereas the thin solid line represents the case of $\rho = 0.3$ mm. The value of F_{σ_w} for $\rho = 0.3$ mm suddenly changes from 0 to 1 when $\sigma_w = 84.7$ MPa, which is due to σ_{w1} and σ_{wd} being cut off by σ_{w2} . In other words, the inhomogeneous particles have almost no effect on the fatigue limit reliability in terms of initiating a fatigue crack. Instead, the eutectic Si actually strengthens the matrix.

Figure 20 shows the relationship between σ_w and $1/\rho$. The solid line represents 50% reliability, the broken line represents 90% reliability, the single-dotted chain line represents 99% reliability, and the open marks represent the experimental results. Because the fatigue limit obtained by the ordinary fatigue test is equivalent to 50% fatigue limit reliability, the solid line agrees well with the open marks. The little differences between the open marks of $\rho = 0.3$ and 0.1 mm and the solid line can be attributed to the fact that ΔK_{wUL} of the present AC4B-T6 was unknown and

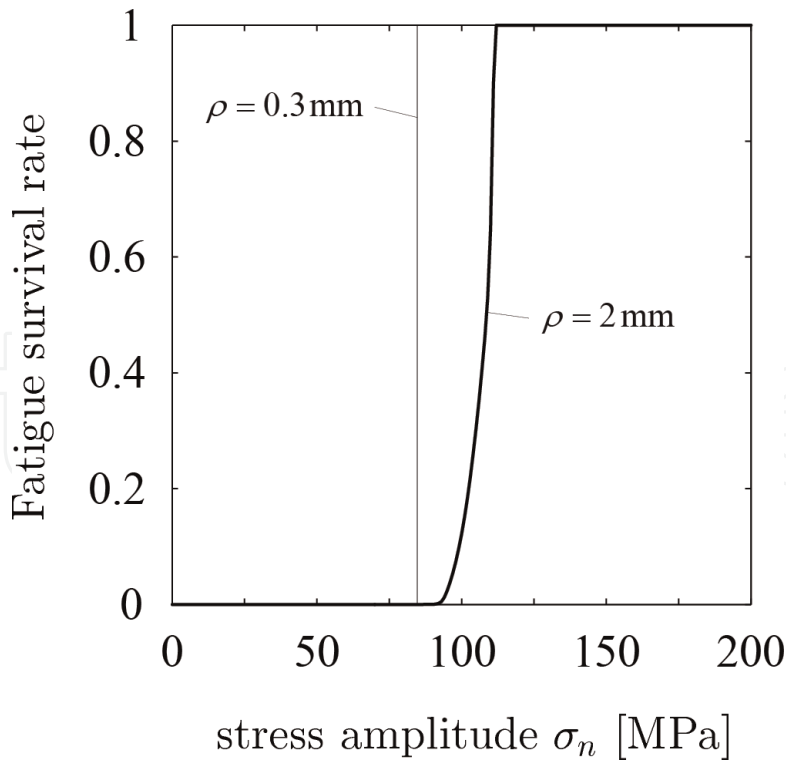


Figure 19.
 Fatigue limit reliability F_{σ_w} .

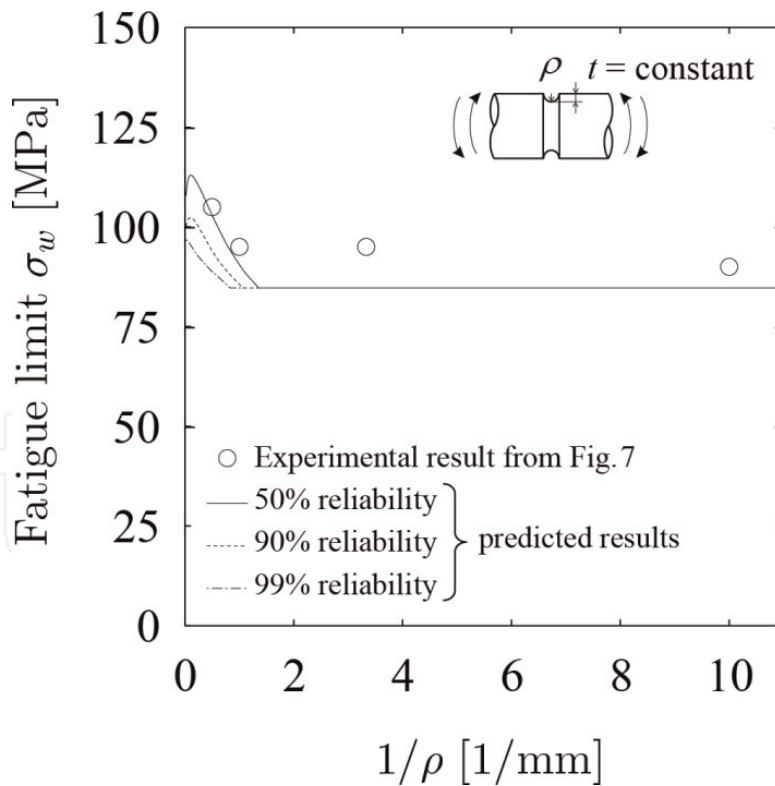


Figure 20.
 Relation between σ_w and $1/\rho$.

the corresponding value for the of Al-Si-X alloy was used for predicting σ_w . It is expected that an even better prediction accuracy would be achieved by using the true ΔK_{wUL} . Nevertheless, σ_w was well predicted, which validated the proposed method for notched AC4B-T6 specimens.

6. Conclusions

This study proposed a nondestructive method for predicting the fatigue limit reliability of notched specimens of a metal containing inhomogeneous particles densely. The method was applied to aluminum cast alloy JIS-AC4B-T6. Rotating-bending fatigue tests were performed on the notched specimens of AC4B-T6 with notch root radius $\rho = 2, 1, 0.3,$ and 0.1 in order to examine the validity of the present method. Since the non-propagating macrocracks were observed along the notch root, the long macrocrack non-propagating limit σ_{w2} appears as the fatigue limit when $\rho = 0.1$ and 0.3 mm. On the other hand, since the non-propagating macrocrack was not observed when $\rho = 1$ and 2 mm, it can be said that the microcrack non-propagating limit σ_{w1} or the small macrocrack non-propagating limit σ_{wd} appears as the fatigue limit. The fatigue limits predicted by the present method were in good agreement with the experimental ones.

The method is not only convenient for use in predicting fatigue strength reliability for the reliable design of machine and structures, but it is also time effective and can be applied to the economic development of materials.

Author details


Tatsujiro Miyazaki¹, Shigeru Hamada² and Hiroshi Noguchi^{2*}

¹ Energy and Environment Program, School of Engineering, University of the Ryukyus, Okinawa, Japan

² Department of Mechanical Engineering, Kyushu University, Fukuoka, Japan

*Address all correspondence to: nogu@mech.kyushu-u.ac.jp

IntechOpen

© 2019 The Author(s). Licensee IntechOpen. This chapter is distributed under the terms of the Creative Commons Attribution License (<http://creativecommons.org/licenses/by/3.0>), which permits unrestricted use, distribution, and reproduction in any medium, provided the original work is properly cited. 

References

- [1] Hébert G, Dubé D, Tremblay R. Tensile and fatigue behaviour of thin-walled cast A383.0 components. *Materials Science and Engineering A*. 2012;**552**:89-96
- [2] Fan KL, He GQ, Liu XS, Liu B, She M, Yuan YL, et al. Tensile and fatigue properties of gravity casting aluminum alloys for engine cylinder heads. *Materials Science and Engineering A*. 2013;**586**(1):78-85
- [3] Hirsch J. Recent development in aluminium for automotive applications. *Transactions of Nonferrous Metals Society of China*. 2014;**24**(7):1995-2002
- [4] Kelly A, Nicholson RB. Precipitation hardening. *Progress in Materials Science*. 1963;**10**:151-391
- [5] Sjo Lander E, Seifeddine S. The heat treatment of Al-Si-Cu-Mg casting alloys. *Journal of Materials Processing Technology*. 2010;**210**:1249-1259
- [6] Shaha SK, Czerwinski F, Kasprzak W, Friedman J, Chen DL. Effect of solidification rate and loading mode on deformation behavior of cast Al-Si-Cu-Mg alloy with additions of transition metals. *Materials Science and Engineering A*. 2015;**636**:361-372
- [7] Kobayashi H, Ikeda H, Murakami Y. Super long life fatigue properties of Al-Si eutectic alloy by rotating-bending and tension-compression fatigue tests. *Transactions of the Japan Society of Mechanical Engineers, Series A*. 1996;**62**(594):347-355. (in Japanese)
- [8] Wang QG, Apelian D, Lados DA. Fatigue behavior of A356/357 aluminum cast alloys. Part II—Effect of microstructural constituents. *Journal of Light Metals*. 2001;**1**(1):85-97
- [9] Lea V-D, Morela F, Belletta D, Saintierb N, Osmondc P. Multiaxial high cycle fatigue damage mechanisms associated with the different microstructural heterogeneities of cast aluminium alloys. *Materials Science and Engineering A*. 2016;**649**(1):426-440
- [10] Laz PJ, Hillberry BM. Fatigue life prediction from inclusion initiated cracks. *International Journal of Fatigue*. 1998;**20**(4):263-270
- [11] Debartolo EA, Hillberry BM. Effects of constituent particle clusters on fatigue behavior of 2024-T3 aluminum alloy. *International Journal of Fatigue*. 1998;**20**(10):727-735
- [12] Miyazaki T, Kang H, Noguchi H, Ogi K. Prediction of high-cycle fatigue life reliability of aluminum cast alloy from statistical characteristics of defects at meso-scale. *International Journal of Mechanical Sciences*. 2008;**50**(2):152-162
- [13] Wang QG, Apelian D, Lados DA. Fatigue behavior of A356-T6 aluminum cast alloys—Part I. Effect of casting defects. *Journal of Light Metals*. 2001;**1**(1):73-84
- [14] Yia JZ, Leea PD, Lindleya TC, Fukuib T. Statistical modeling of microstructure and defect population effects on the fatigue performance of cast A356-T6 automotive components. *Materials Science and Engineering A*. 2006;**432**(1):59-68
- [15] Gao YX, Yi JZ, Lee PD, Lindley TC. The effect of porosity on the fatigue life of cast aluminum-silicon alloys. *Fatigue & Fracture of Engineering Materials & Structures*. 2004;**27**:559-570
- [16] JSME. JSME S 002-1994, Standard Method of Statistical Fatigue Testing. Tokyo, Japan: Japanese Society of

Mechanical Engineering; 1994. (in Japanese)

[17] ISO. ISO12107: Metallic Materials-Fatigue Testing-Statistical Planning and Analysis of Data. Geneva, Switzerland: International Organization for Standardization; 2012

[18] Murakami Y, Endo M. Effects of defects, inclusions and inhomogeneities on fatigue strength. *International Journal of Fatigue*. 1994;**16**:163-182

[19] Murakami Y, Tazunoki Y, Endo T. Existence of the coaxing effect and effects of small artificial holes on fatigue strength of an aluminum alloy and 70-30 brass. *Metallurgical and Materials Transactions A*. 1984;**15**(11):2029-2038

[20] Murakami Y. *Metal Fatigue: Effects of Small Defects and Nonmetallic Inclusions*. Oxford: Elsevier Science Ltd.; 2002

[21] Kobayashi M, Mutsui T. Prediction of fatigue strength of aluminum casting alloys by the $\sqrt{\text{area}}$ parameter model. *Transactions of the Japan Society of Mechanical Engineers, Series A*. 1996; **62**(594):341-346. (in Japanese)

[22] Ceschini L, Morri A, Morri A. Estimation of local fatigue behaviour in A356-T6 gravity die cast engine head based on solidification defects content. *International Journal of Cast Metals Research*. 2014;**27**(1):56-64

[23] Tajiria A, Nozakib T, Uematsub Y, Kakiuchib T, Nakajimac M, Nakamurac Y, et al. Fatigue limit prediction of large scale cast aluminum alloy A356. *Procedia Materials Science*. 2014;**3**: 924-929

[24] Roya MJ, Nadotb Y, Nadot-Martinb C, Bardinb P-G, Maijera DM. Multiaxial Kitagawa analysis of A356-T6. *International Journal of Fatigue*. 2011; **33**(6):823-832

[25] Miyazaki T, Noguchi H, Kage M, Imai R. Estimation for fatigue limit reliability of a metal with inhomogeneities under stress ratio $R = -1$. *International Journal of Mechanical Sciences*. 2005;**47**(2): 230-250

[26] Isibasi T. *Prevention of Fatigue and Fracture of Metals*. Tokyo: Yokendo Ltd.; 1967. (in Japanese)

[27] Nisitani H. Effect of size on the fatigue limit and the branch point in rotary bending tests of carbon steel specimen. *Bulletin of the JSME*. 1968; **11**(47):725-738

[28] Nisitani H, Goto T. Fatigue notch sensitivity of an aluminum alloy. *Transaction of the Japan Society of Mechanical Engineers*. 1976;**42**(361): 2666-2672. (in Japanese)

[29] Nisitani H, Kawagoishi N. Comparison of notch sensitivities in three age-hardened aluminum alloys. *Transaction of the Japan Society of Mechanical Engineers, Series A*. 1985; **51**(462):530-533. (in Japanese)

[30] Takao K, Nisitani H, Sakaguchi H. Relation between crack initiation process and notch sensitivity in rotating bending fatigue. *Journal of the Society of Materials Science, Japan*. 1980; **29**(325):982-987. (in Japanese)

[31] Kawagoishi N, Nisitani H, Tsuno T. Notch sensitivity of squeeze cast aluminum alloy in rotating bending fatigue. *Transaction of the Japan Society of Mechanical Engineers, Series A*. 1990; **56**(521):10-14. (in Japanese)

[32] Dowling NE. Notched member fatigue life predictions combining crack initiation and propagation. *Fatigue & Fracture of Engineering Materials & Structures*. 1979;**2**(2):129-138

[33] Miyazaki T, Noguchi H, Ogi K. Quantitative evaluation of the fatigue

limit of a metal with an arbitrary crack under a stress controlled condition (stress ratio $R = -1$). *International Journal of Fracture*. 2004;**129**:21-38

[34] Miyazaki T, Noguchi H, Kage M. Fatigue limit of steel with an arbitrary crack under a stress controlled constant with a positive mean stress. *International Journal of Fracture*. 2005; **134**:109-126

[35] Miyazaki T, Noguchi H, Kage M. Prediction of fatigue limit reliability of high strength steel with deep notch under mean stress $\sigma_m = 0$. *International Journal of Fracture*. 2011;**168**(1):73-91

[36] Miyazaki T, Noguchi H, Ogi K, Aono Y. Examination of fatigue characteristics of Aluminum cast alloy from meso-level consideration (2nd report, prediction for the fatigue limit reliability of plain specimen of metal containing different sorts of inhomogeneities under $R = -1$). *Transactions of the Japan Society of Mechanical Engineers, Series A*. 2005; **71**(712):1699-1707. (in Japanese)

[37] Hashimoto A, Miyazaki T, Noguchi H, Ogi K. Estimation of particle size distribution in materials in the case of spheroidal particles using quantitative microscopy. *Journal of Testing and Evaluation*. 2000;**28**(5):367-377

[38] Nisitani H. Method of approximate calculation of interference of notch effects and its application. *Bulletin of the JSME*. 1968;**11**(47):725-738

[39] Benthem JP, Koiter WT. Asymptotic approximations to crack problems. In: *Method of Analysis and Solutions of Crack Problems*. Leyden: Noordhoff International; 1973. pp. 131-178